

Is Multiscaling an Artifact in the Stochastically Forced Burgers Equation?

Dhrubaditya Mitra,^{1,2} Jérémie Bec,^{2,3} Rahul Pandit,^{1,*} and Uriel Frisch²

¹Centre for Condensed Matter Theory, Department of Physics,
Indian Institute of Science, Bangalore 560012, India

²Département Cassiopée, Observatoire de la Côte d'Azur, BP4229, 06304 Nice Cedex 4, France

³Dipartimento di Fisica, Università La Sapienza, P.zzle Aldo Moro 2, 00185 Roma, Italy

(Dated: September 3, 2018)

We study turbulence in the one-dimensional Burgers equation with a white-in-time, Gaussian random force that has a Fourier-space spectrum $\sim 1/k$, where k is the wave number. From very-high-resolution numerical simulations, in the limit of vanishing viscosity, we find evidence for multiscaling of velocity structure functions which cannot be falsified by standard tests. We find a new artifact in which logarithmic corrections can appear disguised as anomalous scaling and conclude that bifractal scaling is likely.

PACS numbers: 47.27 Gs, 05.45-a, 05.40-a

Homogeneous, isotropic fluid turbulence is often characterized by the order- p velocity structure functions $S_p(\ell) = \langle \{[\vec{v}(\vec{x} + \vec{\ell}) - \vec{v}(\vec{x})] \cdot (\frac{\vec{\ell}}{\ell})\}^p \rangle$, where $\vec{v}(\vec{x})$ is the velocity at the point \vec{x} and the angular brackets denote an average over the statistical steady state of the turbulent fluid. For separations ℓ in the inertial range, $\eta_d \ll \ell \ll L$, one has $S_p(\ell) \sim \ell^{\zeta_p}$. Here η_d is the small length scale at which dissipation becomes important; L is the large length scale at which energy is fed into the fluid. The 1941 theory (K41) of Kolmogorov [1] predicts *simple scaling* with exponents $\zeta_p^{K41} = p/3$. By contrast, experiments and direct numerical simulations (DNS) suggest *multiscaling* with ζ_p a nonlinear, monotonically increasing, convex function of p , not predictable by dimensional analysis [2]. However, the Reynolds numbers achieved in DNS are limited, so the exponents ζ_p have to be extracted from numerical fits over inertial ranges that extend, at best, over a decade in ℓ . The processing of experimental data – although they can achieve much higher Reynolds numbers – involves other well-known difficulties [3]. It is important therefore to establish, or rule out, multiscaling of structure functions in simpler forms of turbulence, such as passive-scalar, passive-vector or Burgers turbulence. Significant progress, both analytical and numerical, has been made in confirming multiscaling in passive-scalar and passive-vector problems (see, e.g., Ref. [4] for a review). The linearity of the passive-scalar and passive-vector equations is a crucial ingredient of these studies, so it is not clear how they can be generalized to fluid turbulence and the Navier–Stokes equation.

Here we revisit the one-dimensional, Burgers equation with stochastic self-similar forcing, studied earlier in Refs. [5, 6]. It is by far the simplest *nonlinear* partial differential equation (PDE) that has the potential to display multiscaling of velocity structure functions [6]; and it is akin to the Navier–Stokes equation. In particular, we investigate the statistical properties of the solutions

to

$$\partial_t u + u \partial_x u = \nu \partial_{xx} u + f(x, t), \quad (1)$$

in the limit of vanishing viscosity $\nu \rightarrow 0$. Here u is the velocity, and $f(x, t)$ is a zero-mean, space-periodic Gaussian random force with

$$\langle \hat{f}(k_1, t_1) \hat{f}(k_2, t_2) \rangle = 2D_0 |k|^\beta \delta(t_1 - t_2) \delta(k_1 + k_2) \quad (2)$$

and $\hat{f}(k, t)$ the spatial Fourier transform of $f(x, t)$. We restrict ourselves to the case $\beta = -1$ and assume spatial periodicity of period L . Earlier studies [5, 6] suggested that Eqs. (1) and (2), with $\beta = -1$, show a nonequilibrium statistical steady state with *bifractal scaling*: this means that velocity structure functions of order $p \leq 3$ exhibit self-similar scaling with exponents $p/3$ and implies a K41-type $-5/3$ energy spectrum, predictable by dimensional analysis, whereas those of order $p \geq 3$ have exponents all equal to unity being dominated by the finite number of shocks, with $O(L^{1/3})$ strength, typically present in the periodic domain; this bifractal scaling is somewhat similar to that observed when the Burgers equation is forced only at large spatial scales [7, 8].

We overcome the limitations of these earlier studies [5, 6] by adapting the algorithm of Refs. [9, 10] to develop a state-of-the-art technique for the numerical solution of Eqs. (1) and (2), in the $\nu \rightarrow 0$ limit. This yields velocity profiles (Fig. 1 a) with shocks at all length scales resolved. Structure functions [Figs. (1 b) and (1 c)] exhibit power-law behavior over nearly three decades of r ; this is more than two decades better than in Ref. [5]. In principle it should then be possible to measure the scaling exponents [Figs. (1 b)] with enough accuracy to decide between bifractality and multiscaling. A naive analysis [Fig. (2 a)] does suggest multiscaling [15]. However, given that simple scaling or bifractal scaling can sometimes be mistaken for multiscaling in a variety of models [12, 13], it behooves us to check if this is the case here. We describe below our numerical procedure and the various tests we have carried out.

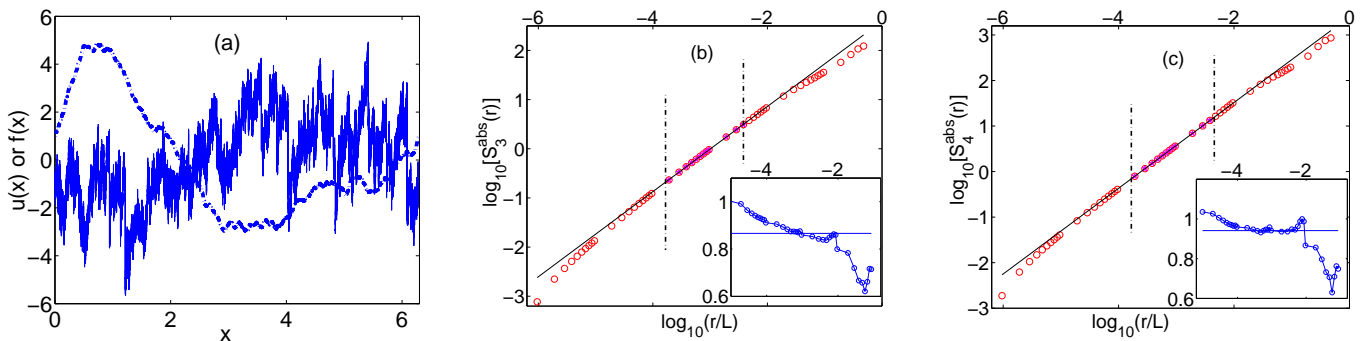


FIG. 1: (a) Representative snapshots of the force f and the velocity u (jagged line), in the statistically stationary régime; the velocity develops small-scale fluctuations much stronger than those present in the force. Log-log plots of the structure function $S_p^{\text{abs}}(r)$ versus r for $N = 2^{20}$ and (b) $p = 3$ and (c) $p = 4$. The straight line indicates the least-squares fit to the range of scales limited by the two vertical dashed lines in the plots. The resulting multiscaling exponents ξ_p (see text) are shown by horizontal lines in the insets with plots of the local slopes versus r .

In our simulations we use $L = 2\pi$ and $D_0 = 1$ without loss of generality. The spatial mesh size is $\delta x = L/N$ where N is the number of grid points. To approximate the forcing, we use the “kicking” strategy of Ref. [9] in which the white-in-time force is approached by shot noise. Between successive kicks we evolve the velocity by using the following well-known result on the solutions to the unforced Burgers equation in the limit of vanishing viscosity (see, e.g., Ref. [8]): the velocity potential ψ (such that $u = -\partial_x \psi$) obeys the maximum principle

$$\psi(x, t') = \max_y \left[\psi(y, t) - \frac{(x-y)^2}{2(t'-t)} \right]; \quad t' > t. \quad (3)$$

The search for the maxima in Eq. (3) requires only $O(N \log_2 N)$ operations [10] because, under Burgers dynamics, colliding Lagrangian particles form shocks and do not cross each other. At small scales we want to have unforced Burgers dynamics with well-identifiable shocks. At least four mesh points are needed for unambiguous identification of a shock; since the maximum wavenumber is $N/2$, we set $\hat{f}(k, t) = 0$ beyond an ultra-violet cutoff $\Lambda = N/8$.

Specifically, at time $t_n = n\delta t$ we add $f_n(x)\sqrt{\delta t}$ to the Burgers velocity $u(x, t)$, where the $f_n(x)$ s are independent Gaussian random functions with zero mean and a Fourier-space spectrum $\sim 1/k$, for $k < \Lambda$. The time step δt is chosen to satisfy the following conditions ($\delta x/2u_0 < \delta t \simeq (1/L\Lambda)^{2/3}(L/u_0)$, where u_0 is the characteristic velocity difference at large length scales $O(L)$). The first ensures that a typical Lagrangian particle moves at least half the mesh-size in time δt (otherwise, it would stay put)[16]; the second, which expresses that δt is comparable to the turnover times at the scale L/Λ , guarantees that, at scales larger than L/Λ the time-step, δt , is small compared to all dynamically significant times, but still permits the formation of individual shocks at smaller scales. Finally, as our simulations are very long, for the stochastic force we use a good-quality random-

Run	N	δt	Λ	τ_L	T_{tr}	T_{av}
B1	2^{20}	5×10^{-4}	2^{17}	1.0	2.0	22
B2	2^{18}	1×10^{-4}	2^{15}	1.0	2.0	20
B3	2^{16}	1×10^{-4}	2^{13}	1.0	2.0	120

TABLE I: Different parameters used in our runs B1, B2 and B3. $\tau_L \equiv L/u_0$ is the equivalent of the large-eddy-turnover time. Data from T_{tr} time steps are discarded so that transients die down. We then average our data over a time T_{av} .

number generator with a long repeat period of 2^{70} due to Knuth [11]. The main characteristics of the runs performed are summarized in Table I.

In addition to the usual structure functions, we have used $S_p^{\text{abs}}(r)$, defined by

$$S_p^{\text{abs}}(r) \equiv \langle |\delta u(x, r)|^p \rangle \sim r^{\xi_p}, \quad (4)$$

$$\delta u(x, r) \equiv u(x+r) - u(x), \quad (5)$$

from which we extract the exponents ξ_p . For each value of N we have calculated ξ_p for $p = m/4$, with integers $1 \leq m \leq 20$. Figure (2 a) summarizes the results of our calculations concerning the exponents ξ_p , for $N = 2^{16}$, 2^{18} , and 2^{20} ; any systematic change in the values of these exponents with N is much less than the error bars determined by the procedure described below. Thus in all other plots we present data from our simulations with $N = 2^{20}$ grid points. The representative log-log plots of Figs. (1 b) and (1 c) of $S_p^{\text{abs}}(r)$ for $p = 3$ and 4 show power-law régimes that extend over nearly three decades of r/L . We obtain our estimates for the exponents ξ_p as follows: for a given value of p we first determine the local slopes of the plot of $\log S_p^{\text{abs}}$ versus $\log r$ by least-squares fits to all triplets of consecutive points deep inside the power-law régime [17]. These regions extend over one and half decade of r/L as shown in Figs. (1 b) and (1 c). The value of ξ_p we quote [Fig. (2 a)] is the mean of these

local slopes; and the error bars shown are the maximum and minimum local slopes in these regions.

Figure (2 a) shows that our results for ξ_p , indicated by circles for $N = 2^{20}$, deviate significantly from the bifractal-scaling prediction (full lines). As we shall see this deviation need not necessarily imply “multiscaling” for the structure functions. We have also considered the possibility of already well-understood artifacts, such as the role of temporal transients [12] and finite-size effects which can round sharp bifractal transitions [13], and decided that they do not play any major role in the present problem [18].

Consider $P^c(s)$, the cumulative probability distribution function of shock strengths s . Simple scaling arguments predict $P^c(s) \sim s^\gamma$, with $\gamma = -3$, which follows by demanding that $P^c(s)$ remain invariant if lengths are scaled by a factor λ and velocities by $\lambda^{-1/3}$. One of the signatures of multiscaling would be deviations of γ from this scaling value. However, the following argument favors $\gamma = -3$: the total input energy, $E_{\text{in}} = \int_{k_0}^{\Lambda} D(k)dk \sim \ln \Lambda$, where Λ is the ultra-violet cutoff. In the limit of vanishing viscosity, the energy dissipation in the Burgers equation occurs only at the shocks and is proportional to the cube of the shock strength [8], so the total energy dissipation is $\Omega \sim \int_{s_{\text{min}}}^{s_{\text{max}}} P(s)s^3 ds$. Here $P(s) = (dP^c(s)/ds) \sim s^{\gamma-1}$ is the probability distribution function (PDF) of shock strengths and s_{min} and s_{max} are, respectively, the minimum and maximum shock strengths. A steady state can occur only if E_{in} and Ω have the same asymptotic properties as $\Lambda \rightarrow \infty$, i.e., $\Omega \sim \ln(\Lambda)$; this requires $\gamma = -3$. By contrast we find $\gamma \simeq -2.7$ [Fig. (2 b)] by a naive least-squares fit to the tail of $P^c(s)$ [19]. This suggests that the results of our simulation are far from the limit $\Lambda \rightarrow \infty$, although more than a million grid points are used. Hence the “anomalous” exponents in Fig. (2 a) might well be suspect.

To explore this further, consider the third-order structure function of velocity differences, without the absolute value, namely, $S_3(r) \equiv \langle \delta u^3 \rangle$. From Eqs. (1) and (2) follows the exact relation

$$\frac{1}{6}S_3(r) = \int_0^r F(y)dy, \quad (6)$$

where $F(y)$ is the spatial part of the force correlation function, defined by $\langle f(x+y, t')f(x, t) \rangle = F(y)\delta(t-t')$. We obtain this analog of the von Kármán–Howarth relation in fluid turbulence by a simple generalization of the proof given in Ref. [9] for the Burgers equation forced deterministically at large spatial scales. An explicit check of Eq. (6) provides a stringent test of our simulations [Fig. (2 c) inset]. Furthermore, Eq. (6) implies that $S_3(r) \sim r \log(r)$ for small r and thus should display significant curvature in a log-log plot, as is indeed seen in Fig. (2 c). By contrast $S_p^{\text{abs}}(r)$ [Fig.(2 c)] displays much less curvature and can be fitted over nearly three decades in (r/L) to a power law with an “anomalous”

exponent of 0.85. This anomalous behavior is probably an artifact as we now show. Let us define the positive (resp., negative) part of the velocity increment δ^+u (resp., δ^-u) equal to δu when $\delta u \geq 0$ and to zero when $\delta u < 0$ (resp., to δu when $\delta u \leq 0$ and to zero when $\delta u > 0$). Obviously $S_3(r) = \langle (\delta^+u)^3 \rangle + \langle (\delta^-u)^3 \rangle$, whereas $S_p^{\text{abs}}(r) = \langle (\delta^+u)^3 \rangle - \langle (\delta^-u)^3 \rangle$. The log-log plot of $\langle (\delta^+u)^3 \rangle = (1/2)[S_3(r) + S_3^{\text{abs}}(r)]$ in Fig. (2 c) is much straighter than those for $S_3(r)$ and $S_3^{\text{abs}}(r)$ and leads to a scaling exponent 1.07 ± 0.02 , very close to unity. For a moment assume that $\langle (\delta^+u)^3 \rangle$ indeed has a scaling exponent of unity. Given that $S_3(r)$ has, undoubtedly, a logarithmic correction, it follows that $S_3^{\text{abs}}(r)$ has (except for a change in sign) the same logarithmic correction in its leading term (for small r) but *differs by a subleading correction proportional to r* . This subleading correction is equivalent to replacing $r \log(r)$ by $r \log(\lambda r)$ for a suitably chosen factor λ . In a log-log plot this shifts the graph away from where it is most curved and thus makes it straighter, albeit with a (local) slope which is not unity.

An independent check of $\langle (\delta^+u)^3 \rangle \sim r$ is obtained by plotting the cumulative probabilities, Φ^c , of positive and negative velocity increments (for a separation $r = 800\delta x$) in Fig. (2 b) [20]. For positive increments Φ^c falls off faster than any negative power of δu , but, for negative ones, there is a range of increments over which $\Phi^c \sim |\delta u|^{-3}$, the same -3 law seen in $P^c(s)$ earlier. Indeed the negative increments are dominated by the contribution from shocks. Just as $P^c(s)$ has cutoffs s_{min} and s_{max} , Φ^c has cutoffs $u_{\text{min}}^-(r)$ and $u_{\text{max}}^-(r)$ for negative velocity increments. Since Φ^c falls off as $|\delta u|^{-3}$, u_{max}^- can be taken to be ∞ ; furthermore as the PDF of velocity differences, $\Phi(\delta u) \equiv d(\Phi^c)/d(\delta u)$, must be normalizable, we find $u_{\text{min}}^-(r) \sim r^{1/3}$. We now know enough about the form of Φ to obtain, in agreement with our arguments above, that $S_3(r) \approx -Ar \ln(r) + Br$ and $S_3^{\text{abs}}(r) \approx Ar \ln(r) + Br$, whence $\langle (\delta^+u)^3 \rangle \approx Br$. The presence of this cutoff yields a logarithmic term in both S_3 and S_3^{abs} but with different sign agreeing with the arguments given in the previous paragraph.

By a similar approach, we find $S_4(r) \approx Cr - Dr^{4/3}$, where C and D are two positive constants. The negative sign before the sub-leading term ($r^{4/3}$) is crucial. It implies that, for any finite r , a naive power-law fit to S_4 can yield a scaling exponent less than unity. The presence of sub-leading, power-law terms with opposite signs also explains the small apparent “anomalous” scaling behavior observed for other values of p in our simulations. A similar artifact involving two competing power-laws has been described in Ref. [14].

In conclusion, we have performed very-high-resolution numerical simulations of the stochastically forced Burgers equation with a $1/k$ forcing spectrum. A naive interpretation of our data shows apparent multiscaling phenomenon. But our detailed analysis has identified a hitherto-unknown numerical artifact by which simple bis-

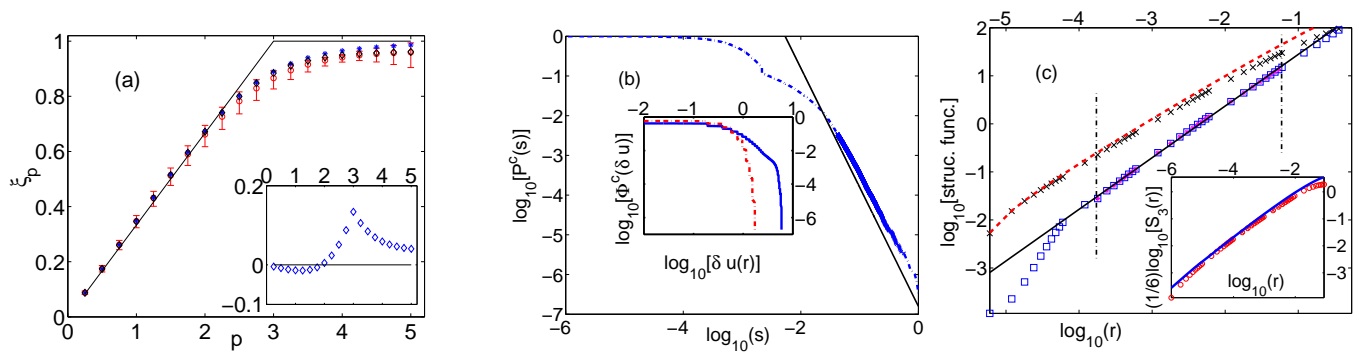


FIG. 2: (a) The multiscaling exponents ξ_p versus order p for Eqs. (1) and (2) with $N = 2^{16}$ (\diamond), 2^{18} ($*$), and 2^{20} (\circ) grid points. Error bars (see text) are shown for the case $N = 2^{20}$. The deviation of ξ_p from the exponents for bifractal scaling (full lines), shown as an inset, suggest naive multiscaling. (b) Log-log plots of the cumulative probability distribution function $P^c(s)$ versus shock strengths s obtained from an average over 1000 snapshots. A least-squares fit to the form $P^c(s) \sim s^\gamma$, for the dark points in the range $-5 \lesssim \log_{10}[P(s)] \lesssim -2.5$, yields $\gamma = -2.70$; the simple-scaling prediction $\gamma = -3$ is indicated by the straight line. The inset shows log-log plots of the cumulative probability distribution function, $\Phi^c[\delta u(r)]$, (dashed line : positive δu , continuous line : negative δu) versus the velocity difference $\delta u(r)$ for length scale $r = 800\delta x$. (c) Log-log plots of $S_3^{\text{abs}}(r)$ (crosses), $S_3^{\text{abs}}(r)$ (dashed line) and $\langle(\delta^+u)^3\rangle$ (squares) versus r . The continuous line is a least-square fit to the range of points limited by two vertical dashed lines in the plot. Inset: An explicit check of Eq. (6) from our simulations, plotted on a log-log scale. The dashed line is the right-hand side of Eq. (6); the left-hand side of this equation has been obtained for $N = 2^{20}$ (\circ) (run B1).

caling can masquerade as multiscaling. Our work illustrates that the elucidation of multiscaling in spatially extended nonlinear systems, including the Navier–Stokes equation, requires considerable theoretical insight that must supplement state-of-the-art numerical simulations and experiments.

We thank E. Aurell, L. Biferale, A. Lanotte, and V. Yakhot for discussions. This research was supported by the Indo-French Centre for the Promotion of Advanced Research (Project 2404-2), by CSIR (India), and by the European Union under contracts HPRN-CT-2000-00162 and HPRN-CT-2002-00300. Additional computational resources were provided by CHEP (IISc).

* Also at Jawaharlal Nehru Centre For Advanced Scientific Research, Jakkur, Bangalore, India

- [1] A.N. Kolmogorov, *Dokl. Acad. Nauk USSR* **30**, 9 (1941).
- [2] U. Frisch, *Turbulence: The Legacy of A.N. Kolmogorov* (Cambridge University Press, Cambridge, 1996).
- [3] F. Anselmet, Y. Gagne, E.J. Hopfinger and R.A. Antonia *J. Fluid. Mech.* **140**, 63 (1984) and references therein.
- [4] G. Falkovich, K. Gawędzki, and M. Vergassola, *Rev. Mod. Phys.* **73**, 913 (2001) and references therein.
- [5] A. Chekhlov and V. Yakhot, *Phys. Rev. E* **52**, 5681 (1995).
- [6] F. Hayot and C. Jayaprakash, *Phys. Rev. E* **56**, 4259 (1997); *ibid*, **56**, 227 (1997).
- [7] W. E, K. Khanin, A. Mazel and Ya. Sinai, *Phys. Rev. Lett.* **78**, 1904 (1997).
- [8] U. Frisch and J. Bec in *New Trends in Turbulence*, A. Yaglom, F. David, and M. Lesieur eds., Les Houches Session

LXXIV (Springer EDP-Sciences, 2001) p 341.

- [9] J. Bec, U. Frisch, and K. Khanin, *J. Fluid Mech.* **416**, 239 (2000).
- [10] A. Noullez and M. Vergassola, *J. Sci. Comp.* **9**, 259 (1994).
- [11] D.E. Knuth, *The Art of Computer Programming*, Vol. 2 (Addison Wesley Longman, Singapore, 1999) pp. 184–187. P. Grassberger, *New J. Phys.* **4**, 17 (2002).
- [12] A. Kundagrami and C. Dasgupta, *Physica A*, **270**, 135 (1999).
- [13] E. Aurell, U. Frisch, A. Noullez and M. Blank, *J. Stat. Phys.*, **88**, 1151 (1997).
- [14] L. Biferale, M. Cencini, A.S. Lanotte, M. Sbragaglia and F. Toschi, *New J. Phys.* **6**, 37 (2004).
- [15] In Ref. [6] the authors argued that Eqs. (1) and (2), with $-1 < \beta < 0$, could lead to *genuine multifractality*. Their results, obtained by a pseudospectral DNS with a finite viscosity, had a scaling range far smaller than can be achieved now. Our results for values of β in this range will be reported elsewhere.
- [16] This condition is opposite to the Courant–Friedrich–Lewy-type condition, which is not needed with our algorithm
- [17] Deviations from this power-law régime occur at small values of r because of the ultraviolet cutoff Λ for the stochastic force (2).
- [18] Details on such questions can be found in the earlier version of the present paper, available at <http://xxx.lanl.gov/abs/nlin.CD/0406049v1>
- [19] To estimate shock locations we look at groups of four grid points where the discretized velocity gradient changes its sign twice (they correspond to a “zig-zag” in the velocity profile).
- [20] Similar plots from lower-resolution viscous spectral simulations were obtained in Ref. [5].